Detecting Massive Scalar Fields with Extreme Mass-Ratio Inspirals

Susanna Barsanti,[1,2] Andrea Maselli,[3,4] Thomas P. Sotiriou,[5,6] and Leonardo Gualtieri[7]
[1]Dipartimento di Fisica, "Sapienza" Università di Roma, Piazzale Aldo Moro 5, 00185 Roma, Italy
[2]Sezione INFN Roma1, Roma 00185, Italy
[3]Gran Sasso Science Institute (GSSI), I-67100 L'Aquila, Italy
[4]INFN, Laboratori Nazionali del Gran Sasso, I-67100 Assergi, Italy
[5]School of Mathematical Sciences and School of Physics and Astronomy, University of Nottingham, University Park, Nottingham, NG7 2RD, United Kingdom
[6]Nottingham Centre of Gravity, University of Nottingham, University Park, Nottingham NG7 2RD, United Kingdom
[7]Dipartimento di Fisica, Università di Pisa and Sezione INFN Pisa, Largo Bruno Pontecorvo 3, 56127 Pisa, Italy

(Received 20 December 2022; revised 4 April 2023; accepted 25 May 2023; published 3 August 2023)

We study the imprint of light scalar fields on gravitational waves from extreme mass-ratio inspirals—binary systems with a very large mass asymmetry. We first show that, to leading order in the mass ratio, any effects of the scalar on the waveform are captured fully by two parameters: the mass of the scalar and the scalar charge of the secondary compact object. We then use this theory-agnostic framework to show that the future observations by LISA will be able to *simultaneously* measure both of these parameters with enough accuracy to detect ultralight scalars.

DOI: 10.1103/PhysRevLett.131.051401

Introduction.—Asymmetric binaries represent a new family of compact sources of gravitational waves (GWs) with an exceptional discovery potential. Mildly asymmetric binaries have already been observed by LIGO, VIRGO, and KAGRA Collaborations (LVK) [1]. LISA [2] is expected to observe compact binaries with much lower mass ratios, up to a factor of 10^5. These sources can lie in the detection band for years, rather than minutes, because in the final stages of the inspiral the evolution timescale of a highly asymmetric binary is proportional to the mass ratio. The large number of gravitational wave cycles produced while the smaller (secondary) object is performing relativistic orbits around the larger (primary) object is expected to offer unprecedented precision in parameter estimation for astrophysics [3–15] and fundamental physics [16–31] alike.

Extreme mass-ratio inspirals (EMRIs), in which a stellar-mass secondary of mass m_p evolves around a supermassive black hole (BH) of mass M with mass ratios of $q = m_p/M \sim 10^{-3} - 10^{-6}$, are perhaps the most promising sources in this respect. In particular, they can be a very sensitive probe of new fundamental scalar fields [17,32–38]. Scalars are ubiquitous in cosmological models of dark energy and/or dark matter and in extension of the standard model (SM) or general relativity (GR) [16,39].

Harnessing the potential of asymmetric binaries, and EMRIs in particular, for detecting or constraining new fundamental fields requires developing accurate waveforms in scenarios that include such fields. Remarkably, for massless scalars, it was shown in Ref. [35] that this can be done in a theory-agnostic way to leading order in the mass ratio. Any (self-)interaction of the scalar that respects shift symmetry—the symmetry that protects the scalar from acquiring a mass—affects the waveform only through a single parameter: the scalar charge per unit mass of the secondary d. This framework was used in Ref. [36] to produce the first forecasts for LISA's ability to detect scalar charge.

It is worth stressing that massive scalars are expected to leave an observable imprint on compact objects only if their Compton wavelength, the inverse of their mass, is comparable to the wavelength of the emitted GW, i.e., to the length scale of the source [40]. In geometrical ($G = c = 1$) units, if M is the length scale of the source (e.g., for a BH system, the BH mass) and $\mu_s\hbar$ is the scalar-field mass, the condition is roughly $\mu_s M \lesssim 1$. We note that [41]

$$\mu_s[\mathrm{eV}] \simeq \left(\frac{\mu_s M}{0.75}\right)\left(\frac{10^6 M_\odot}{M}\right)10^{-16}\ \mathrm{eV}. \tag{1}$$

Hence, the scalars that GW observations can currently probe would have masses smaller than $\sim 10^{-16}$ eV (ultralight scalar fields; see, e.g., Ref. [42], and references therein).

Nonetheless, the assumption of a strictly vanishing mass and of shift symmetry, as in Ref. [35], can be too restrictive. Certain scenarios, such as superradiance-induced clouds [41] or scalarization [43–47], rely on the presence of a mass or of interactions that violate shift symmetry to generate scalar charge. Moreover, measuring the mass of an ultralight scalar is in itself an exciting prospect. Indeed, significant effort has already been put into constraining the mass of scalar fields using pulsar or LVK observations; see, e.g., Refs. [40,42,48,49].

The main goal of this Letter is to demonstrate that EMRIs are sensitive probes of ultralight scalar fields, which can allow us to measure the scalar charge per unit mass of the secondary and the mass of the scalar field *simultaneously*, and with impressive precision.

Setup.—We consider the general action

$$S[\mathbf{g},\varphi,\Psi] = S_0[\mathbf{g},\varphi] + \alpha S_c[\mathbf{g},\varphi] + S_m[\mathbf{g},\varphi,\Psi], \quad (2)$$

where

$$S_0 = \int d^4x \frac{\sqrt{-g}}{16\pi}\left(R - \frac{1}{2}\partial_\mu\varphi\partial^\mu\varphi - \frac{1}{2}\mu_s^2\varphi^2\right), \quad (3)$$

where R is the Ricci scalar and μ_s is the mass of the scalar field. S_c encodes all additional interaction of the scalar field, including nonminimal couplings to gravity, and is assumed to be analytic in φ. S_m describes matter fields. In an EMRI the secondary object can be treated as a point particle, by replacing S_m with the "skeletonized action" [50],

$$S_p = -\int m(\varphi)\sqrt{g_{\alpha\beta}\frac{dy_p^\alpha}{d\lambda}\frac{dy_p^\beta}{d\lambda}}d\lambda, \quad (4)$$

where $m(\varphi)$ is a scalar function. By varying Eq. (2) with respect to $\mathbf{g}$ and φ, we obtain the field equations:

$$G_{\mu\nu} = -\frac{16\pi\alpha}{\sqrt{-g}}\frac{\delta S_c}{\delta g^{\mu\nu}} + 8\pi T^{\rm scal}_{\mu\nu} + 8\pi T^{p}_{\mu\nu}, \quad (5)$$

$$(\Box - \mu_s^2)\varphi = -\frac{8\pi\alpha}{\sqrt{-g}}\frac{\delta S_c}{\delta\varphi} + 16\pi\frac{\delta S_p}{\delta\varphi}, \quad (6)$$

where $T^{\rm scal}_{\mu\nu}$ is the standard scalar-field stress-energy tensor and $T^{p}_{\mu\nu}$ is the stress-energy tensor for S_p. Equations (5) and (6) can be solved perturbatively in $q = m_p/M \ll 1$, with the secondary acting as a perturbation of the massive BH background.

We assume that α has negative mass dimensions in units where $c = \hbar = 1$ (i.e., it suppresses irrelevant operators), or positive length dimensions in the $G = c = \hbar = 1$ geometric units that we use here. Then following Ref. [35] one can relate α to q as follows: $\alpha/M^n = (\alpha/m_p^n)q^n$, where n is a positive integer. As already stated in the Introduction, we focus on scalar masses that satisfy $\mu_s M \leq 1$, as heavier scalars are not expected to leave any imprint on EMRIs. This implies that $\mu_s m_p \ll 1$ and the scalar is far from being confined at scales m_p. The fact that it has not been already detected by observation of black holes of a few solar masses or in weak field [51] implies that α/m_p^n is not much larger than 1. The $\alpha = 0$ case in particular is covered by no-hair theorems [52,53] and hence the primary would be a Kerr black hole with $\varphi = 0$. Combining all of the above, one can treat the deviations from the Kerr metric and the EMRI dynamics perturbatively, with q as a single bookkeeping parameter. When $\mu_s M \ll 1$, the mass of the scalar can be neglected and one recovers the results of Ref. [35], while when $\mu_s M$ becomes O(1) it is essential to include its contribution, as we do below.

We will only consider quantities to leading order in the mass ratio. Hence $T^{\rm scal}_{\mu\nu}$ and $\delta S_c/\delta\varphi$, which are quadratic in q, can be neglected. The scalar perturbation φ_1 is then fully determined by the secondary. In a buffer region close to the secondary, small enough to be inside its world tube, but far away such that the metric can be considered as a perturbation of flat spacetime, Eq. (6) reduces to

$$(\Box - \mu_s^2)\varphi_1 = 0, \quad (7)$$

whose solution, in a reference frame $\{\tilde{x}_\mu\}$ centered on the particle, has the form

$$\varphi_1 \simeq \frac{m_p d}{\tilde{r}}e^{-\mu_s\tilde{r}} + O\left(\frac{m_p^2}{\tilde{r}^2}e^{-\mu_s\tilde{r}}\right), \quad (8)$$

where d is the scalar charge of the secondary. By matching Eq. (8) with the solution of Eq. (6) in the buffer region, we find that $m(0) = m_p$ and $m'(0)/m(0) = -d/4$.

Equations (5) and (6) can then be written as

$$G^{\alpha\beta} = 8\pi m_p\int\frac{\delta^{(4)}(x - y_p(\lambda))}{\sqrt{-g}}\frac{dy_p^\alpha}{d\lambda}\frac{dy_p^\beta}{d\lambda}d\lambda, \quad (9)$$

$$(\Box - \mu_s^2)\varphi = -4\pi d m_p\int\frac{\delta^{(4)}(x - y_p(\lambda))}{\sqrt{-g}}d\lambda, \quad (10)$$

where we have replaced explicit expressions for $T^p_{\mu\nu}$ and $\delta S_p/\delta\varphi$, and y_p^μ identifies the worldline followed by the secondary. Equations (9) and (10) are solved perturbatively following the Teukolsky approach [54]. The scalar field is decomposed in spheroidal harmonics as a sum over multipoles (ℓ, m). Details on the scalar perturbations are given in the Supplemental Material [55].

The total energy loss emitted by both the scalar and the gravitational sector is the sum of the contributions at the horizon and at infinity:

$$\dot{E}_{\rm GW} = \sum_{i=+,-}[\dot{E}^i_{\rm grav} + \dot{E}^i_{\rm scal}] = \dot{E}_{\rm grav} + \dot{E}_{\rm scal}, \quad (11)$$

where the dot indicates the time derivative. Since the source term of the scalar-field equation depends linearly on the

charge, the scalar energy flux can be written as $\dot{E}_{\rm scal} = d^2\dot{\tilde{E}}_{\rm scal}$, such that $q^{-2}\dot{\tilde{E}}_{\rm scal}$ only depends on $(r/M, a/M, \mu_s M)$.

The flux at infinity identically vanishes for frequencies smaller than the scalar-field mass, $\omega < \mu_s$. This is a typical behavior for massive scalar fields (see, e.g., Refs. [49,56,57]. Therefore, for every combination of (ℓ, m) a specific radius r_s exists such that for $r > r_s$ the energy flux at infinity vanishes. This suppression may lead to nondetectable imprints in the GW emission, as we will discuss in our analysis. The general behavior of the scalar energy flux as a function of the orbital radius and of μ_s is discussed in the Supplemental Material [55].

Unlike the emission at infinity, the flux at horizon is present for each value of the orbital frequency, and contributes to the binary's orbital evolution throughout the entire inspiral. Moreover it shows a new important feature, the appearance of resonances, which are not present if the scalar field is massless.

Resonances occur when the binary orbital frequencies are comparable with those of the scalar quasinormal modes of the BH background spacetime. In this case the energy emission grows toward a peak which can be either positive or negative depending on the BH spin and on the superradiance condition $\omega < m\Omega_h$, where $\Omega_h = a/(2Mr_h)$ and $r_h = M + \sqrt{M^2 - a^2}$. If the peak is negative, the scalar radiation can be strong enough to counterbalance the gravitational emission, giving rise to floating orbits [33,58]. Determining whether floating orbits persist at postadiabatic level or how quickly the secondary moves through a resonance requires self-force calculations [33], which are beyond the scope of this Letter. Hereafter, we neglect resonances, which is a rather conservative approach. Taking them into account is expected to make the waveform more distinguishable from an EMRI waveform in GR and hence improve parameter estimation and our ability to detect a new scalar.

The gravitational and the massless scalar fluxes have been computed by making use of the Black Hole Perturbation Toolkit [59], while for the massive scalar fluxes we developed a *Mathematica* code, publicly available [60], together with tabulated values of $q^{-2}\dot{\tilde{E}}^{\pm}_{\rm scal}$ as a function of $(r/M, a/M, \mu_s M)$. Further details on the implementation are given in the Supplemental Material [55].

The energy emission drives the EMRI orbital evolution and, in the adiabatic approximation, the balance law between the binary binding energy and the GW flux $\dot{E} = -\dot{E}_{\rm GW}$ allows us to compute the change in the orbital parameters, i.e., the radial and the azimuthal coordinates (r, ϕ). We set the initial phase ϕ_0 to zero and the initial radius r_0 such that the EMRI evolves until the secondary reaches a plunging radius of $0.1M$ from the innermost stable circular orbit in $T = 1$ yr.

We model the emitted time-dependent gravitational waveform in the quadrupole approximation, finding the GW strain measured by the detectors $h(t, \vec{\theta}) = F_+ h_+ + F_\times h_\times$. This quantity depends on 12 parameters $\vec{\theta} = (\ln M, \ln m_p, \chi, d, \bar{\mu}_s, r_0, \phi_0, \theta_s, \phi_s, \theta_l, \phi_l, d_L)$, where d_L is the source luminosity distance, $\chi = a/M$ is the dimensionless spin parameter, and $\bar{\mu}_s = \mu_s M$. The LISA orbital motion is taken into account by the time-dependent pattern functions $F_{+,\times}$ which depend on the binary orientation (θ_s, ϕ_s) and the spin direction (θ_l, ϕ_l) in a solar barycentric frame (see Ref. [36] for further details on the waveform modeling and implementation).

Given two templates $h_{1,2}$, we define their inner product:

$$\langle h_1 | h_2 \rangle = 4\mathrm{Re} \int_{f_{\rm min}}^{f_{\rm max}} \frac{\tilde{h}_1(f)\tilde{h}_2^\star(f)}{S_n(f)} df, \tag{12}$$

where $\tilde{h}(f)$ is the Fourier transform of the time-domain signal, the $\star$ superscript identifies complex conjugation, and S_n is the LISA power spectral density, which includes the confusion noise of unresolved white-dwarf binaries [61]. The signal-to-noise ratio (SNR) of a given waveform h_1 is then given by $\rho = \langle h_1 | h_1 \rangle^{1/2}$. We also define the faithfulness between two templates,

$$\mathcal{F}[h_1, h_2] = \max_{\{t_c, \Phi_c\}} \frac{\langle h_1 | h_2 \rangle}{\sqrt{\langle h_1 | h_1 \rangle \langle h_2 | h_2 \rangle}}, \tag{13}$$

with (t_c, Φ_c) time and phase offsets. This quantity provides an estimate of how much two waveforms differ, weighted by the detector sensitivity. We assume that for a SNR $\rho = 30$, two signals are distinguishable if $\mathcal{F} \lesssim \mathcal{F}_{\rm thr} = 0.994$ [62].

In the limit of large SNR, the posterior distribution of $\vec{\theta}$ inferred by an EMRI detection can be approximated by a Gaussian centered around the true values $\vec{\bar{\theta}}$, with covariance $\mathbf{\Sigma} = \mathbf{\Gamma}^{-1}$, where $\Gamma_{ij} = \langle (\partial h/\partial\theta_i) | (\partial h/\partial\theta_j) \rangle_{\vec{\theta}=\vec{\bar{\theta}}}$ is the Fisher information matrix, whose diagonal element $\sigma_i = \Sigma_{ii}^{1/2}$ corresponds to the statistical error of the ith parameter, and $c_{\theta_i\theta_j} = \Sigma_{ij}/\sigma_{\theta_i}\sigma_{\theta_j}$ is the correlation coefficient between the parameters θ_i, θ_j [63]. For the waveform models which include both the scalar charge and the field's mass, we obtain 12×12 Fisher matrices computed by varying the all set of parameters $\vec{\theta}$. In this approach the SNR scales linearly with the inverse of the luminosity distance. Hereafter, we scale d_L in order to have binaries with $\rho = 150$, which is in the range of the expected SNRs of EMRI detections by LISA [64].

Results.—We first study the distinguishability between the baseline GR model, i.e., assuming $(d, \bar{\mu}_s) = (0, 0)$, and waveforms with nonvanishing values of the charge and of the scalar field mass. The top panel of Fig. 1 shows the faithfulness between the "plus" polarization h_+ computed in these two scenarios, for EMRIs with secondary mass of one and ten solar masses, as a function of d and $\bar{\mu}_s$.

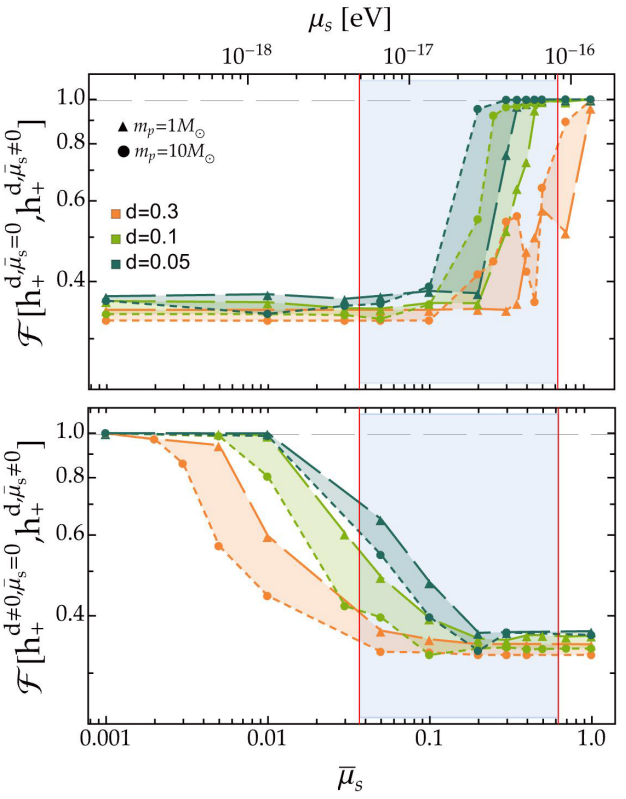

FIG. 1. Top: faithfulness between a GW signal with "plus" polarization with $d = 0$ and one with $d \neq 0$, $\bar{\mu}_s \neq 0$ for 12 months of observation before the plunge. We fix the primary mass and spin to $M = 10^6 M_\odot$ and $\chi = 0.9$, respectively, while considering different values m_p and d. The shaded region corresponds to the range of scalar-field masses which could be excluded by superradiance bounds (courtesy of Brito). Bottom: faithfulness between two signals with the same value of $d \neq 0$, one having $\bar{\mu}_s = 0$ and the other with $\bar{\mu}_s \neq 0$. The horizontal dashed line corresponds to the threshold value $\mathcal{F}_{\rm thr}$. We consider the same EMRI configurations as in the top panel.

As previously discussed, large values of $\bar{\mu}_s$ tend to suppress the GW flux at infinity, and hence the overall dissipative contribution of the scalar sector, as the energy emission at the horizon is subdominant.

Indeed, the faithfulness deteriorates rapidly as the scalar-field mass decreases. For $0.05 < d < 0.1$, it lies below $\mathcal{F}_{\rm thr}$ for $\bar{\mu}_s \lesssim 0.3$ for the binaries we considered. Larger values of the scalar charge ($d = 0.3$) allow the two waveforms to be distinguishable for more massive scalar configurations, with $\bar{\mu}_s \gtrsim 0.7$. For a lighter secondary the faithfulness appears to reach $\mathcal{F}_{\rm thr}$ at a larger $\bar{\mu}_s$. However, the $d = 0.3$ case is an outlier in this respect and also exhibits some additional peaks and troughs for larger values of $\bar{\mu}_s$, which persists for larger values of d. The corresponding fluxes do not exhibit any remarkable difference from those corresponding to lower values of d or $\bar{\mu}_s$, so it is not clear what causes these changes in the faithfulness for larger values of d and $\bar{\mu}_s$. Numerical errors were analyzed by varying the precision of the fluxes which serve as input parameters for the faithfulness computations. The results are stable under large increase of the flux precision, and are presented in Table 2 of the Supplemental Material [55].

We also note that for $\bar{\mu}_s \lesssim 0.03$ ($\mu_s \lesssim 4 \times 10^{-18}$ eV), the GR and the scalar waveforms are clearly distinguishable, with $\mathcal{F} \lesssim 0.4$, regardless of the charge. Such estimates are complementary to other bounds which are expected to provide information on the existence of scalar fields in the gravity sector from future astrophysical probes. As an example, in both panels of Fig. 1 we draw as shaded regions the parameter space which can be potentially ruled out by superradiance constraints inferred from observations of massive BH binaries [41]. Our results suggest that, depending on d, EMRIs provide a new powerful channel to constrain both light and heavy fields, which do not fall within the superradiance window.

As a step forward in this analysis we exploit the faithfulness to assess the minimum $\bar{\mu}_s$ which can be distinguished from the massless case. The bottom panel of Fig. 1 shows indeed the values of $\mathcal{F}$ computed between the gravitational waveform with plus polarization with either $\bar{\mu}_s = 0$ or $\bar{\mu}_s \neq 0$ and fixed scalar charge. We consider the same binaries analyzed in the top panel. Our results show that, for charges as small as $d \sim 0.05$, LISA could be able to distinguish fields with $\bar{\mu}_s \gtrsim 0.01$ ($\mu_s \sim 10^{-18}$ eV) from their massless counterpart. This bound is larger by almost an order of magnitude if $d \gtrsim 0.3$.

The analysis developed so far, however, takes only partially into account the correlations between the waveform parameters, which could hamper our ability to reconstruct the charge and the mass of the scalar field. The actual detectability of such parameters requires a more sophisticated analysis, based on the Fisher matrix approach, which fully takes into account the correlations among the GW parameters. We apply the latter to LISA observations of prototype EMRIs injecting $M = 10^6 M_\odot$, $\chi = 0.9$, $\theta_s = \phi_s = \pi/2$, $\theta_l = \phi_l = \pi/4$, $d = 0.1$ and considering four values of $m_p = (1.4, 4.6, 10, 15) M_\odot$ and two values of $\bar{\mu}_s = (0.018, 0.036)$, which lie outside the superradiance window highlighted in Fig. 1, and for which the flux at infinity is significant throughout the entire inspiral.

The joint and marginal posterior distributions on $\bar{\mu}_s$ and d derived for these systems are shown in the left- and right-hand columns of Fig. 2, respectively. A summary of the 1σ uncertainties inferred for $\bar{\mu}_s$ and d is reported in Table I, together with their correlation coefficients, which show how $\bar{\mu}_s$ and d are strongly (anti)correlated.

Errors on d decrease as the mass ratio m_p/M increases, for both values of $\bar{\mu}_s$. Binaries with $m_p \gtrsim 10 M_\odot$ are able to exclude the $d = 0$ case at more than 90% credible level. For the EMRI configuration with $m_p = 4.6 M_\odot$, errors slightly deteriorate, with the null scenario ruled out at 1σ. Constraints on $\bar{\mu}_s$ show more variability. For the lowest injected value, $\bar{\mu}_s = 0.018$, errors follow the same

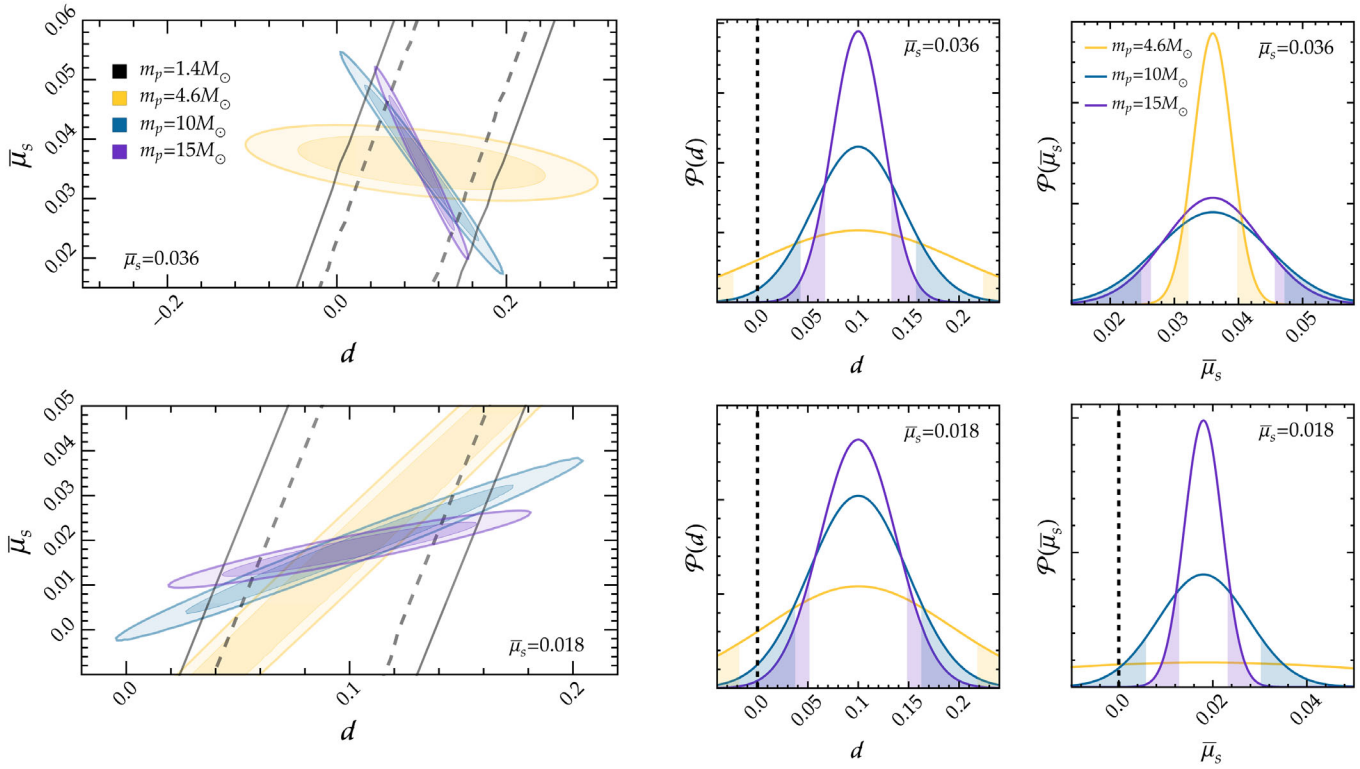

FIG. 2. Left: credible intervals at 68% and 90% for the joint posterior distribution of the charge d and the scalar field mass $\bar{\mu}_s$. We consider EMRIs with injected parameters $d = 0.1$, $M = 10^6 M_\odot$, $a = 0.9M$, different values of the secondary mass, $\bar{\mu}_s = 0.036$ (top row), and $\bar{\mu}_s = 0.018$ (bottom row). Right: marginal distributions for d and $\bar{\mu}_s$. The white area between shaded regions provides 90% of the probability distribution. The vertical dashed lines identify the GR scenario with $d = \bar{\mu}_s = 0$.

hierarchy observed for the scalar charge, with the measurement accuracy improving for heavier secondaries. In this setup, however, $\bar{\mu}_s$ remains unconstrained for the EMRI with $m_p = 4.6 M_\odot$. This picture changes completely for the $\bar{\mu}_s = 0.036$ case, in which the strongest bound is led by the lightest secondary. Binaries with $m_p = 10 M_\odot$ and $m_p = 15 M_\odot$ provide larger, and almost identical, errors. The dependence on such results on the secondary mass is mostly dictated by two ingredients: (i) correlations among the scalar charge and the field's mass and (ii) the EMRI orbital configuration within the observational window we have considered, which spans one year of evolution until the plunge. Very light secondaries start their inspiral at smaller initial radii, where the scalar flux has a smaller relative contribution compared to the dominant quadrupolar mode, and the signal features a very slow evolution with little variation in the frequency content.

TABLE I. 1σ relative uncertainties and correlation coefficients on the charge and on the scalar-field mass for the configurations shown in Fig. 2. We assume $d = 0.1$ for all the binaries.

m_p ($M_\odot$)	$\bar{\mu}_s$	σ_d/d (%)	$\sigma_{\bar{\mu}_s}/\bar{\mu}_s$ (%)	$c_{d\bar{\mu}_s}$
1.4	0.018	345	2364	0.997
	0.036	363	391	0.992
4.6	0.018	92	243	0.995
	0.036	97	8	−0.485
10	0.018	49	53	0.984
	0.036	45	24	−0.990
15	0.018	38	22	0.938
	0.036	26	21	−0.986

In comparison with the massless case, where the relative error on the scalar charge for the binary with $m_p = 10 M_\odot$ is $\simeq$4% [36], here it is larger: $\sigma_d/d \simeq 45\%$ and 49% for $\bar{\mu}_s = 0.036$ and $\bar{\mu}_s = 0.018$, respectively. This is expected due to correlations with $\bar{\mu}_s$ which enters now as an additional parameter. Nevertheless, in all cases in which the probability distribution of $\bar{\mu}_s$ is constrained by the data, we are able to exclude the massless scenario at more than 90% credible level.

Discussion.—Our results provide the first direct analysis on the capability of EMRI observations by the future space interferometer LISA to detect massive scalar fields and simultaneously measure the mass of the scalar and the scalar charge of the secondary. Our analysis assumes that the primary is adequately described by the Kerr spacetime at leading order in the mass ratio. We have shown, using no-hair theorems [52,53] and effective field theory arguments [35], that this is quite generically a valid assumption, provided that the primary is a black hole. Indeed our setup is theory agnostic, and changes in the binary evolution are

uniquely determined by the scalar charge per unit mass of the EMRI secondary d and by the scalar-field mass μ_s. Therefore, ready-to-use templates for parameter estimation and phenomenological studies can be straightforwardly generated for a vast range of beyond-GR and beyond-standard-model scenarios that contain a new massive scalar.

We have exploited such waveforms to assess the combined effect of nonvanishing d and μ_s. By computing the faithfulness between signals from uncharged and charged secondaries, we have shown that ultralight scalar fields can leave a strong imprint on the GW emission, potentially detectable by LISA for a wide range of binary configurations. In particular, our results show how EMRIs provide a new observational window, complementary to other astrophysical probes, for detecting or constraining ultralight scalar fields.

We have performed a parameter estimation on prototype EMRI signals to further investigate the constraints that LISA will place on the scalar charge and on field's mass. Our results suggest that LISA will be able to measure, with a single event, *both* d and μ_s accurately enough to potentially confirm the existence of an ultralight scalar field at more than 90% confidence level. A limitation of the analysis leading to this result is that it has focused on equatorial circular inspirals and certain simplifying approximations.

Indeed, realistic EMRIs are expected to follow more complex trajectories along inclined and eccentric orbits. The effects of inclination are currently under investigation [65], while the inclusion of eccentricity is expected to further enhance the distinguishability between signals with and without a scalar field [38,66]. Moreover, the scalar field emission exhibits some level of degeneracy with astrophysical signatures of different origin, such as environmental effects due to gravitational drag or accretion [8]. We expect, however, correlations between the latter and the scalar charge or mass to be small, so long as they carry a different GW frequency content within the waveform evolution.

Improvements to our work would also include using fully relativistic GW templates, performing a Bayesian analysis, and including postadiabatic terms which take into account self-force corrections [67]. Considering the effects of resonances [33] is also expected to further increase the distinguishability against GR signals, thus strengthening the results of our analysis. Finally, it would be interesting to extend our analysis to vector fields.

This work makes use of the Black Hole Perturbation Toolkit. The authors would like to acknowledge networking support by the COST Action CA16104. T. P. S. acknowledges partial support from the STFC Consolidated Grants No. ST/T000732/1 and No. ST/V005596/1. L. G. acknowledges financial support from the EU Horizon 2020 Research and Innovation Programme under the Marie Sklodowska-Curie Grant Agreement No. 101007855.

[1] R. Abbott *et al.* (LIGO Scientific, VIRGO, and KAGRA Collaborations), GWTC-3: Compact binary coalescences observed by LIGO and Virgo during the second part of the third observing run, arXiv:2111.03606.
[2] P. Amaro-Seoane *et al.* (LISA Collaboration), Laser interferometer space antenna, arXiv:1702.00786.
[3] P. A. Seoane *et al.*, The effect of mission duration on LISA science objectives, Gen. Relativ. Gravit. **54**, 3 (2022).
[4] D. Laghi, N. Tamanini, W. Del Pozzo, A. Sesana, J. Gair, S. Babak, and D. Izquierdo-Villalba, Gravitational-wave cosmology with extreme mass-ratio inspirals, Mon. Not. R. Astron. Soc. **508**, 4512 (2021).
[5] C. P. L. Berry, S. A. Hughes, C. F. Sopuerta, A. J. K. Chua, A. Heffernan, K. Holley-Bockelmann, D. P. Mihaylov, M. C. Miller, and A. Sesana, The unique potential of extreme mass-ratio inspirals for gravitational-wave astronomy, arXiv:1903.03686.
[6] S. McGee, A. Sesana, and A. Vecchio, Linking gravitational waves and x-ray phenomena with joint LISA and Athena observations, Nat. Astron. **4**, 26 (2020).
[7] P. Amaro-Seoane, J. R. Gair, M. Freitag, M. Coleman Miller, I. Mandel, C. J. Cutler, and S. Babak, Astrophysics, detection and science applications of intermediate- and extreme mass-ratio inspirals, Classical Quantum Gravity **24**, R113 (2007).
[8] V. Cardoso and A. Maselli, Constraints on the astrophysical environment of binaries with gravitational-wave observations, Astron. Astrophys. **644**, A147 (2020).
[9] E. Barausse, V. Cardoso, and P. Pani, Can environmental effects spoil precision gravitational-wave astrophysics?, Phys. Rev. D **89**, 104059 (2014).
[10] N. Yunes, B. Kocsis, A. Loeb, and Z. Haiman, Imprint of Accretion Disk-Induced Migration on Gravitational Waves from Extreme Mass Ratio Inspirals, Phys. Rev. Lett. **107**, 171103 (2011).
[11] B. Kocsis, N. Yunes, and A. Loeb, Observable signatures of EMRI black hole binaries embedded in thin accretion disks, Phys. Rev. D **84**, 024032 (2011).
[12] K. Destounis, A. G. Suvorov, and K. D. Kokkotas, Gravitational-Wave Glitches in Chaotic Extreme-Mass-Ratio Inspirals, Phys. Rev. Lett. **126**, 141102 (2021).
[13] V. Cardoso, K. Destounis, F. Duque, R. Panosso Macedo, and A. Maselli, Gravitational Waves from Extreme-Mass-Ratio Systems in Astrophysical Environments, Phys. Rev. Lett. **129**, 241103 (2022).
[14] P. S. Cole, G. Bertone, A. Coogan, D. Gaggero, T. Karydas, B. J. Kavanagh, T. F. M. Spieksma, and G. M. Tomaselli, Disks, spikes, and clouds: Distinguishing environmental effects on BBH gravitational waveforms, arXiv:2211.01362.
[15] J. Bamber, J. C. Aurrekoetxea, K. Clough, and P. G. Ferreira, Black hole merger simulations in wave dark matter environments, Phys. Rev. D **107**, 024035 (2023).
[16] L. Barack *et al.*, Black holes, gravitational waves and fundamental physics: A roadmap, Classical Quantum Gravity **36**, 143001 (2019).
[17] E. Barausse *et al.*, Prospects for fundamental physics with LISA, Gen. Relativ. Gravit. **52**, 81 (2020).
[18] E. Barausse, N. Yunes, and K. Chamberlain, Theory-Agnostic Constraints on Black-Hole Dipole Radiation with

Multiband Gravitational-Wave Astrophysics, Phys. Rev. Lett. **116**, 241104 (2016).
[19] J. L. Blázquez-Salcedo, C. F. B. Macedo, V. Cardoso, V. Ferrari, L. Gualtieri, F. S. Khoo, J. Kunz, and P. Pani, Perturbed black holes in Einstein-dilaton-Gauss-Bonnet gravity: Stability, ringdown, and gravitational-wave emission, Phys. Rev. D **94**, 104024 (2016).
[20] K. Glampedakis and S. Babak, Mapping spacetimes with LISA: Inspiral of a test-body in a 'quasi-Kerr' field, Classical Quantum Gravity **23**, 4167 (2006).
[21] L. Barack and C. Cutler, Using LISA EMRI sources to test off-Kerr deviations in the geometry of massive black holes, Phys. Rev. D **75**, 042003 (2007).
[22] V. Cardoso, G. Castro, and A. Maselli, Gravitational Waves in Massive Gravity Theories: Waveforms, Fluxes and Constraints from Extreme-Mass-Ratio Mergers, Phys. Rev. Lett. **121**, 251103 (2018).
[23] S. Datta, R. Brito, S. Bose, P. Pani, and S. A. Hughes, Tidal heating as a discriminator for horizons in extreme mass ratio inspirals, Phys. Rev. D **101**, 044004 (2020).
[24] P. Pani and A. Maselli, Love in extrema ratio, Int. J. Mod. Phys. D **28**, 1944001 (2019).
[25] E. Maggio, M. van de Meent, and P. Pani, Extreme mass-ratio inspirals around a spinning horizonless compact object, Phys. Rev. D **104**, 104026 (2021).
[26] K. Destounis, A. G. Suvorov, and K. D. Kokkotas, Testing spacetime symmetry through gravitational waves from extreme-mass-ratio inspirals, Phys. Rev. D **102**, 064041 (2020).
[27] G. A. Piovano, A. Maselli, and P. Pani, Model independent tests of the Kerr bound with extreme mass ratio inspirals, Phys. Lett. B **811**, 135860 (2020).
[28] L. Annulli, V. Cardoso, and R. Vicente, Stirred and shaken: Dynamical behavior of boson stars and dark matter cores, Phys. Lett. B **811**, 135944 (2020).
[29] N. Sago and T. Tanaka, Oscillations in the extreme mass-ratio inspiral gravitational wave phase correction as a probe of a reflective boundary of the central black hole, Phys. Rev. D **104**, 064009 (2021).
[30] G. A. Piovano, A. Maselli, and P. Pani, Constraining the tidal deformability of supermassive objects with extreme mass ratio inspirals and semianalytical, frequency-domain waveforms, Phys. Rev. D **107**, 024021 (2023).
[31] H.-K. Guo, K. Sinha, and C. Sun, Probing boson stars with extreme mass ratio inspirals, J. Cosmol. Astropart. Phys. 09 (2019) 032.
[32] P. Pani, V. Cardoso, and L. Gualtieri, Gravitational waves from extreme mass-ratio inspirals in dynamical Chern-Simons gravity, Phys. Rev. D **83**, 104048 (2011).
[33] N. Yunes, P. Pani, and V. Cardoso, Gravitational waves from quasicircular extreme mass-ratio inspirals as probes of scalar-tensor theories, Phys. Rev. D **85**, 102003 (2012).
[34] O. A. Hannuksela, K. W. K. Wong, R. Brito, E. Berti, and T. G. F. Li, Probing the existence of ultralight bosons with a single gravitational-wave measurement, Nat. Astron. **3**, 447 (2019).
[35] A. Maselli, N. Franchini, L. Gualtieri, and T. P. Sotiriou, Detecting Scalar Fields with Extreme Mass Ratio Inspirals, Phys. Rev. Lett. **125**, 141101 (2020).
[36] A. Maselli, N. Franchini, L. Gualtieri, T. P. Sotiriou, S. Barsanti, and P. Pani, Detecting fundamental fields with LISA observations of gravitational waves from extreme mass-ratio inspirals, Nat. Astron. **6**, 464 (2022).
[37] L. G. Collodel, D. D. Doneva, and S. S. Yazadjiev, Equatorial extreme-mass-ratio inspirals in Kerr black holes with scalar hair spacetimes, Phys. Rev. D **105**, 044036 (2022).
[38] S. Barsanti, N. Franchini, L. Gualtieri, A. Maselli, and T. P. Sotiriou, Extreme mass-ratio inspirals as probes of scalar fields: Eccentric equatorial orbits around Kerr black holes, Phys. Rev. D **106**, 044029 (2022).
[39] E. Berti *et al.*, Testing general relativity with present and future astrophysical observations, Classical Quantum Gravity **32**, 243001 (2015).
[40] J. Antoniadis *et al.*, A massive pulsar in a compact relativistic binary, Science **340**, 6131 (2013).
[41] R. Brito, V. Cardoso, and P. Pani, Superradiance: New frontiers in black hole physics, Lect. Notes Phys. **906**, 1 (2015).
[42] R. Brito, S. Ghosh, E. Barausse, E. Berti, V. Cardoso, I. Dvorkin, A. Klein, and P. Pani, Gravitational wave searches for ultralight bosons with LIGO and LISA, Phys. Rev. D **96**, 064050 (2017).
[43] T. Damour and G. Esposito-Farese, Nonperturbative Strong Field Effects in Tensor-Scalar Theories of Gravitation, Phys. Rev. Lett. **70**, 2220 (1993).
[44] H. O. Silva, J. Sakstein, L. Gualtieri, T. P. Sotiriou, and E. Berti, Spontaneous Scalarization of Black Holes and Compact Stars from a Gauss-Bonnet Coupling, Phys. Rev. Lett. **120**, 131104 (2018).
[45] D. D. Doneva and S. S. Yazadjiev, New Gauss-Bonnet Black Holes with Curvature-Induced Scalarization in Extended Scalar-Tensor Theories, Phys. Rev. Lett. **120**, 131103 (2018).
[46] A. Dima, E. Barausse, N. Franchini, and T. P. Sotiriou, Spin-Induced Black Hole Spontaneous Scalarization, Phys. Rev. Lett. **125**, 231101 (2020).
[47] D. D. Doneva, F. M. Ramazanoğlu, H. O. Silva, T. P. Sotiriou, and S. S. Yazadjiev, Scalarization, arXiv:2211.01766.
[48] K. Yamada, T. Narikawa, and T. Tanaka, Testing massive-field modifications of gravity via gravitational waves, Prog. Theor. Exp. Phys. **2019**, 103E01 (2019).
[49] F. M. Ramazanoğlu and F. Pretorius, Spontaneous scalarization with massive fields, Phys. Rev. D **93**, 064005 (2016).
[50] D. M. Eardley, Observable effects of a scalar gravitational field in a binary pulsar, Astrophys. J. **196**, L59 (1975).
[51] R. Nair, S. Perkins, H. O. Silva, and N. Yunes, Fundamental Physics Implications for Higher-Curvature Theories from Binary Black Hole Signals in the LIGO-Virgo Catalog GWTC-1, Phys. Rev. Lett. **123**, 191101 (2019).
[52] J. D. Bekenstein, Novel "no-scalar-hair" theorem for black holes, Phys. Rev. D **51**, R6608 (1995).
[53] T. P. Sotiriou and V. Faraoni, Black Holes in Scalar-Tensor Gravity, Phys. Rev. Lett. **108**, 081103 (2012).
[54] S. A. Teukolsky, Perturbations of a rotating black hole. 1. Fundamental equations for gravitational electromagnetic and neutrino field perturbations, Astrophys. J. **185**, 635 (1973).
[55] See Supplemental Material at http://link.aps.org/supplemental/10.1103/PhysRevLett.131.051401 for detailed information on the scalar perturbations, on the

implementation of the codes for the EMRI energy emission and parameter estimation, as well as a study of the Fisher matrices stability and of the parameter estimation with the inclusion of multipoles larger then the dipole for the scalar flux.

[56] J. Alsing, E. Berti, C. M. Will, and H. Zaglauer, Gravitational radiation from compact binary systems in the massive Brans-Dicke theory of gravity, Phys. Rev. D **85**, 064041 (2012).

[57] E. Berti, L. Gualtieri, M. Horbatsch, and J. Alsing, Light scalar field constraints from gravitational-wave observations of compact binaries, Phys. Rev. D **85**, 122005 (2012).

[58] V. Cardoso, S. Chakrabarti, P. Pani, E. Berti, and L. Gualtieri, Floating and Sinking: The Imprint of Massive Scalars Around Rotating Black Holes, Phys. Rev. Lett. **107**, 241101 (2011).

[59] Black Hole Perturbation Toolkit, http://bhptoolkit.org/.

[60] SGREP Repo, https://github.com/masellia/SGREP/.

[61] T. Robson, N. J. Cornish, and C. Liu, The construction and use of LISA sensitivity curves, Classical Quantum Gravity **36**, 105011 (2019).

[62] K. Chatziioannou, A. Klein, N. Yunes, and N. Cornish, Constructing gravitational waves from generic spin-precessing compact binary inspirals, Phys. Rev. D **95**, 104004 (2017).

[63] M. Vallisneri, Use and abuse of the Fisher information matrix in the assessment of gravitational-wave parameter-estimation prospects, Phys. Rev. D **77**, 042001 (2008).

[64] S. Babak, J. Gair, A. Sesana, E. Barausse, C. F. Sopuerta, C. P. L. Berry, E. Berti, P. Amaro-Seoane, A. Petiteau, and A. Klein, Science with the space-based interferometer LISA. V: Extreme mass-ratio inspirals, Phys. Rev. D **95**, 103012 (2017).

[65] M. Della Rocca *et al.* (to be published).

[66] C. Zhang, Y. Gong, D. Liang, and B. Wang, Gravitational waves from eccentric extreme mass-ratio inspirals as probes of scalar fields, arXiv:2210.11121.

[67] L. Speri *et al.*, Fast EMRI waveforms to test general relativity (to be published).